ACS OMEGA

http://pubs.acs.org/journal/acsodf

Article

Evaporation-Induced Diffusion Acceleration in Liquid-Filled Porous Materials

Xuefeng Wang, Pengpeng Jia, Shanyouming Sun, Xiaocong He, Tian Jian Lu, Feng Xu, and Shangsheng Feng*

Cite This: *ACS Omega* 2021, 6, 21646−21654

Read Online

ACCESS | Metrics & More | Article Recommendations | Supporting Information

ABSTRACT: Liquid-filled porous materials exist widely in nature and engineering fields, with the diffusion of substances in them playing an important role in system functions. Although surface evaporation is often inevitable in practical scenarios, the evaporation effects on diffusion behavior in liquid-filled porous materials have not been well explored yet. In this work, we performed noninvasive diffusion imaging experiments to observe the diffusion process of erioglaucine disodium salt dye in a liquid-filled nitrocellulose membrane under a wide range of relative humidities (RHs). We found that evaporation can significantly accelerate the diffusion rate and alter concentration distribution compared with the case without evaporation. We explained the accelerated diffusion phenomenon by the mechanism that evaporation would induce a weak flow in liquid-filled porous materials, which leads to convective diffusion, *i.e.*, evaporation-induced flow and diffusion (EIFD). Based on the EIFD mechanism, we proposed a convective diffusion model to quantitatively predict the diffusion process in liquid-filled porous materials under evaporation and experimentally validated the model. Introducing the dimensionless Peclet (P_e) number to measure the relative contribution of the evaporation effect to pure molecular diffusion, we demonstrated that even at a high RH of 95%, where the evaporation effect is usually assumed negligible in common sense, the evaporation-induced diffusion still overwhelms the molecular diffusion. The flow velocity induced by evaporation in liquid-filled porous materials was found to be 0.4−5 μm/s, comparable to flow in many biological and biomedical systems. The present analysis may help to explain the driving mechanism of tissue perfusion and provide quantitative analysis or inspire new control methods of flow and material exchange in numerous cutting-edge technologies, such as paper-based diagnostics, hydrogel-based flexible electronics, evaporation-induced electricity generation, and seawater purification.

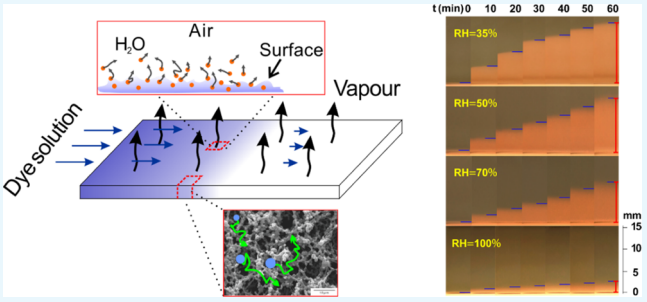

1. INTRODUCTION

Porous materials are a wide class of heterogeneous materials composed of solid skeletons and pores filled with gas or liquid or both. In particular, liquid-filled porous materials are common in nature and engineering applications, such as native tissues (*e.g.*, liver, bone), biomaterials (*e.g.*, wood, hydrogel, soil), engineering materials (*e.g.*, metallic foam), *etc.*[1] The diffusion of substances, such as biomolecules and nanoparticles, in liquid-filled porous materials is related to a number of cutting-edge technologies, such as treatment of soil pollutants,[2] thermochemical heat storage system,[3] drug transport in biological tissues,[4] gel chromatography separation,[5,6] and point-of-care testing (POCT).[7−9] The diffusion process is vital for the abovementioned applications, which can be tailored to either increase or decrease the diffusion rate. For example, in cases of filter membranes[10] and size-exclusion chromatography,[11] the rate of the diffusion process should be slowed down to ensure that the molecules pass through the porous medium slowly. Nevertheless, in other cases, such as porous bionic materials,[12] targeted therapy with antineoplastic drugs,[4] and resource extraction,[13−16] the rate of mass transfer needs to be accelerated. Understanding the diffusion process of substances inside liquid-filled porous materials could reveal the working principle and underlying mechanisms of various natural and engineering problems and provide guidance for improving materials design or achieve new disease treatment methods.

The diffusion process in a homogeneous solution is governed by the Fick's law, with its rate determined by the diffusion coefficient.[17] According to the relationship between pore size (d) and average free path (λ) of random thermal motion of diffusing molecules, the diffusion of substances in a liquid-filled porous material can be divided into the Fick

Received: June 9, 2021
Accepted: July 30, 2021
Published: August 11, 2021

https://doi.org/10.1021/acsomega.1c03052
ACS Omega 2021, 6, 21646−21654

diffusion ($d \geq 100\ \lambda$), the Knudsen diffusion ($d \geq 10\ \lambda$), and the transition zone diffusion.[18] For the latter two cases, a collision between molecules and pore framework determines the migration rate of molecules in the liquid-filled porous material,[19−22] such as single-file diffusion (SFD) of protein drugs through nanochannels[23] and confined diffusion of finite-size particles in periodic nanostructures.[19,22] In these cases, the spatial accessibility of diffusion particles depends on the relative size of the channel and particles.

For Fick diffusion in a liquid-filled porous material, the size-exclusion effect of pore on diffusing molecules can be ignored because the pore size is typically much larger than the free path of diffusing molecules.[24] The liquid-filled porous material is then equivalent to a homogeneous liquid, and the equivalent diffusion coefficient D_{eff} can be introduced to measure the diffusion rate.[18] Previous studies have focused on the influence of the pore structure (*e.g.*, porosity φ, tortuosity τ), adsorption, chemical reactions, temperature, and the properties of diffusing molecules on D_{eff}. A number of liquid-filled porous materials (*e.g.*, gels,[25,26] silica film,[27−29] foam dressing,[30] nitrocellulose (NC) membranes[31]) have been extensively investigated. For example, a single-particle tracking method was employed to study fluorescent terrylene diimide (TDI) molecules in a hexagonal mesoporous silica film,[27] and the orientations of pores were found to determine the direction of particle diffusion. A diffusion imaging method was adopted to study the diffusion of avidin fluorescein particles in hydroxyethyl methacrylate/methacrylic acid (HEMA/MAA) hydrogels,[6] and adsorption was found to significantly reduce the effective diffusion coefficient by three orders of magnitude. Meanwhile, the influence of temperature on D_{eff} was also quantified: increasing the temperature significantly increases the diffusion rate of substances in hydrogels.[2,25]

Liquid evaporation from the surface of a porous material is inevitable and exists widely in natural and engineering problems, such as test paper, hydrogels, and foam dressings. Surface evaporation from a microfluidic system causes two main functions: fluid transport and material exchange.[32] For example, evaporation would limit the radial permeability of liquid in porous media,[33] control the wetting behavior of liquid on the surface,[34−36] and cause the "coffee ring" effect in ink-jet printing.[37−39] Evaporation-induced water flow within a porous carbon sheet can drive ions through the narrow porous gap and generate voltage,[40−42] which may be used for physiological information monitoring.[40,43] In energy and environmental applications, evaporation accelerates salt transport in salt marshes;[44] for a hydrogel-based evaporator, water evaporates through the surface of the gel, which promotes the separation of Na^+, Cl^- and pure water, thus realizing seawater purification.[14,45−49] In biomedical engineering, surface evaporation from foam dressing affects the rate of wound healing due to changes in moisture permeability and internal nutrient transfer.[30] During the storage and use of flexible electronic materials, evaporation affects the distribution of the electrolyte concentration in hydrogels, thus changing the conductivity of the material and its functions.[50,51] Further, evaporation was found to reduce the speed of wicking flow in paper-based diagnostics.[52−54] Given that the diffusion time scale is much larger than that of wicking flow, the change of wicking flow by evaporation should influence the diffusion process.[9] In fact, environmental relative humidity (RH) and temperature were found to strongly affect the signal intensity of lateral flow assays (LFAs),[55] where a RH beyond 60% with temperatures of 55−60 and 37−40 °C produces optimum nucleic acid hybridization and antigen−antibody interaction in LFAs. Although evaporation-induced diffusion in liquid-filled porous materials is common and important, the phenomenon is yet to be systematically and quantitatively investigated. There is also no theoretical framework to describe the diffusion process.

In this study, evaporation-induced flow and diffusion (EIFD) in liquid-filled porous NC membranes was discovered through noninvasive diffusion imaging experiments. We hypothesized that the accelerated diffusion is attributed to evaporation-induced flow in liquid-filled NC membranes, causing convective diffusion. Based on this assumption, a convective diffusion model was adopted to describe the diffusion process with evaporation, validated by experiments performed under different humidity environments. Combining the experiment and theory, we quantified the effects of evaporation on the flow velocity, the diffusion rate, and the diffusion profile. We further discussed the significance of the EIFD mechanism from both science and engineering perspectives. Our study may shed light on explaining the driving mechanism of tissue perfusion and inspire new control methods of flow and material exchange in liquid-filled porous materials for various cutting-edge technologies.

2. EXPERIMENTAL METHODS

2.1. Experimental Setup and Materials. We built an experiment platform using poly(methyl methacrylate) (PMMA) to visualize the diffusion process, including an external environmental box, a microenvironment chamber, test sample, dye pool, temperature and humidity probes, linear traverse, and a digital camera, as shown in Figure 1a. The test sample was placed in the microenvironmental chamber made of PMMA, which was fixed to a U-frame. The U-frame was connected to a one-dimensional (1-D) linear traverse, which was programmable to move with an accuracy of 0.076 mm, thus enabling precise control of the immersion depth of the test sample into the dye pool. To avoid evaporation, the dual

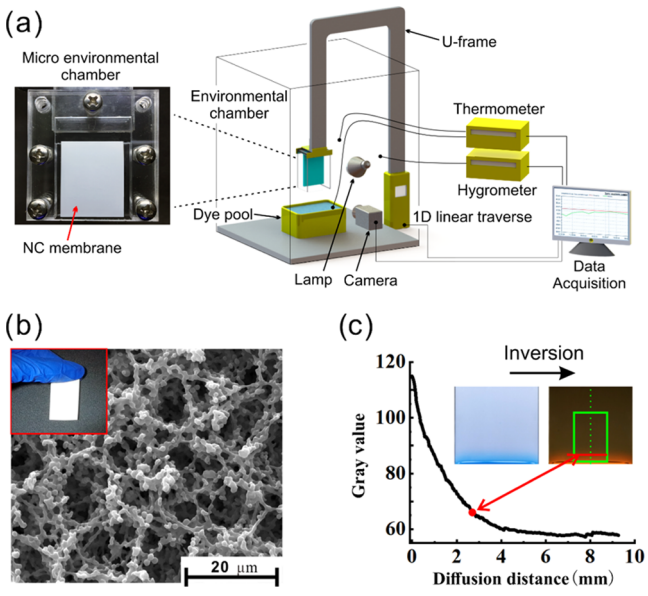

Figure 1. Experimental methods: (a) experimental setup, (b) SEM image of NC membranes, and (c) conversion from the diffusion image to concentration distribution of the diffusing substance.

https://doi.org/10.1021/acsomega.1c03052
ACS Omega 2021, 6, 21646−21654

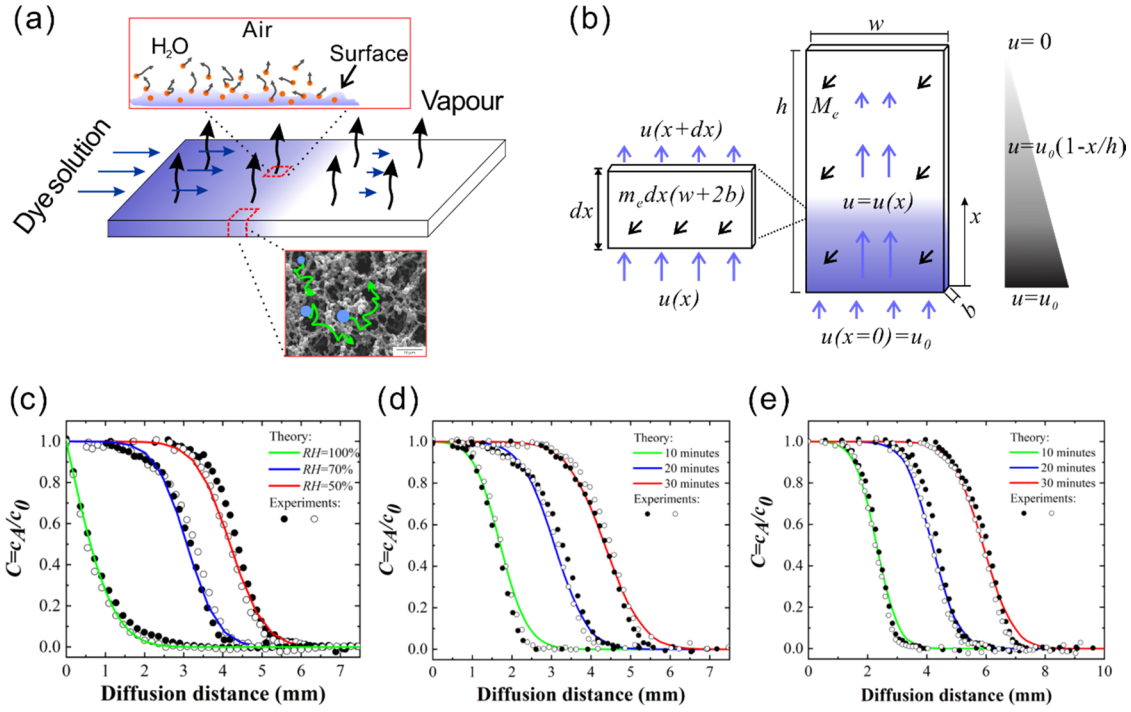

Figure 2. Theoretical model and verification: (a) schematics of flow diffusion caused by evaporation on the surface of the liquid-filled porous material and (b) determination of the evaporative flow velocity by analyzing the mass conservation of liquid over an infinitesimal element length; comparison between the experimental and simulated concentration distributions along the diffusion direction: (c) at given diffusion time t = 20 min with three different RHs, (d) at given RH = 70% with different diffusion times, and (e) at given RH = 50% with different diffusion times.

environmental chambers were designed to achieve ∼100% humidity near the test sample. By adjusting the opening degree of the external and the microenvironmental chambers, air humidity around the test sample could be stably controlled, allowing for a wide range of test humidities, from 35% (atmosphere humidity) to ∼100%. Air temperature in the external environmental box was maintained the same as that of the dye pool (21 ± 1 °C), both monitored using T-type thermocouples. Air humidity in the external environmental box was measured with a humidity meter.

The tested porous material was NC membranes (HFC07502/HFC13502), with a porosity of φ = 0.906 and a pore size of d = 8.323 μm for HFC07502 and φ = 0.866 and d = 4.909 μm for HFC13502,[56] as shown in Figure 1b. The NC membrane is widely used as a substrate material in diagnostic devices, such as lateral flow assay tests (LFAs),[57] where a plastic film on its back is designed by the manufacturer to facilitate the use and storage but does not affect the diffusion process.

Erioglaucine disodium salt, with a molecular formula of $C_{37}H_{34}N_2Na_2O_9S_3$, was used as a diffusing substance in the experiments. According to Samprovalaki et al.[58] who used the diffusion imaging method to study diffusion in hydrogels, the sensitivity of conversion from the gray to concentration value increases with decreasing concentration of the dye solution because at a higher concentration, the fluctuation of the gray value produces larger errors when the system is saturated. Therefore, in the present experiments, the concentration of erioglaucine disodium salt was fixed at 0.2 mg/mL, which had been calibrated to ensure accuracy of the diffusion imaging method.

Each NC membrane specimen was tested under varying environmental humidities to investigate how evaporation affects the diffusion rate. During each test, upon achieving steady temperature and humidity in the environmental chamber, the specimen was immersed into the dye pool to initiate the diffusion process. The entire diffusion process was then recorded using a digital camera, with a fixed frame rate of 50 fps and a resolution of 1920 × 1080.

2.2. Diffusion Imaging Processing. Original diffusion images from a digital camera were first converted into gray images and then reversed between the white and black colors. In the 256-bit color order, white corresponds to a color intensity of 0 and black corresponds to 256, which is the basis for calculating the concentration distribution of dyes in NC membranes. As shown in Figure 1c, to avoid the edge effect and the influence of light reflection on the boundary, we selected the middle area as the region of interest to extract the gray value distribution, from a diffusion source point to an infinite distance along each NC membrane. By averaging the gray value on a horizontal line in the region of interest, the average gray value at a certain x position was calculated using ImageJ software. Then, conversion from a gray value to concentration can be carried out, using the following formula

$$\frac{c_A}{c_0} = \frac{G_A - G}{G_0 - G} \quad (1)$$

where c_A is the concentration at position x, c_0 is the initial concentration at the origin, G_A is the gray value of position x at time t, G is the background gray value, and G_0 is the gray value at the source point.

3. THEORY

A theoretical model was established below, based on the following assumptions: (1) the diffusion belongs to dilute solution diffusion so the diffusion coefficient is independent of

https://doi.org/10.1021/acsomega.1c03052
ACS Omega 2021, 6, 21646−21654

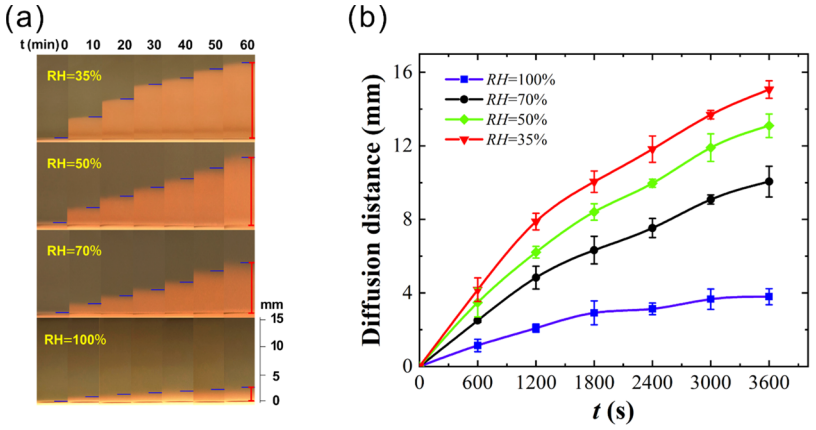

Figure 3. Experimental results for the diffusion of erioglaucine disodium salt dye in the liquid-filled NC membrane (HFC13502) under selected relative humidity: (a) diffusion images and (b) diffusion distances varying with time.

the concentration, (2) one-dimensional (1-D) diffusion holds along the length of the NC membrane, (3) concentration of diffusion dye at the origin is constant, and (4) diffusion dye can not reach the other end of the sample within the period of interest, so the process can be described using a 1-D semi-infinite model.

With environmental relative humidity RH = 100%, no evaporation occurs at the surface of the NC membrane. In the case of pure diffusion without evaporation, the classic 1-D semi-infinite diffusion model can be adopted to predict the concentration distribution shown as follows[2,59]

$$\frac{\partial c_A}{\partial t} = D_{eff}\frac{\partial^2 c_A}{\partial x^2} \tag{2}$$

Analytic solution of eq 2 gives concentration distribution of dye along the NC membrane given as follows[60]

$$\frac{c_A}{c_0} = \mathrm{erfc}\left(\frac{x}{2\sqrt{tD_{eff}}}\right) \tag{3}$$

where D_{eff} is the effective diffusion coefficient, which can be obtained by fitting the experimental data of pure diffusion according to eq 3, as shown in Section 1 of the Supporting Information.

However, under an evaporative environment, our experiment data showed that the classic theory for pure diffusion failed to predict the concentration distribution, with the diffusion rate significantly increased compared to pure diffusion. To explain and quantify evaporation effects, we have to modify the classic theory to account for the presence of evaporation. To this end, we assumed that surface evaporation would cause a weak flow in the liquid-filled NC membrane, thus producing convective diffusion. When the surrounding air is not saturated by liquid vapors, as the liquid-containing pores on the surface of the NC membrane are exposed to the surrounding atmosphere, the liquid in the pores evaporates to the environment. To compensate for the liquid loss caused by evaporation, the solution flows through the liquid-filled NC membrane from the source upward, as shown in Figure 2a.

Figure 2a displays schematics of evaporation-induced flow in an NC membrane, where $x = 0$ represents the location of the source solution. As shown in Figure 2b, upon considering an infinitesimal length element dx along the diffusion direction, the conservation of mass in the element leads to

$$u(x)\rho wb\varphi = u(x + \mathrm{d}x)\rho wb\varphi + m_e \mathrm{d}x(w + 2b) \tag{4}$$

$$\frac{\mathrm{d}u}{\mathrm{d}x}\mathrm{d}x\rho wb\varphi = -m_e \mathrm{d}x(w + 2b) \tag{5}$$

Solution of eq 5 with the boundary condition of $u'_{x=0} = u_0$ shows that the flow velocity in the NC membrane caused by evaporation decreases linearly along the diffusion direction, given by

$$u = -\frac{m_e(w + 2b)}{\rho bw\varphi}x + u_0 \tag{6}$$

where ρ is the density of water, φ, w, and b are the porosity, width, and thickness of the NC membrane, respectively, and m_e is the evaporation flux, which can be determined by separate numerical simulations[61−64] or from empirical correlations,[53] as shown in Section 2 of the Supporting Information.

Let u_0 represent the flow velocity at the root of the NC membrane. As evaporation loss of water from the whole liquid-filled NC membrane is compensated at the root, conservation of mass dictates that

$$u_0 = \frac{m_e h(w + 2b)}{\rho w\varphi b} \tag{7}$$

Upon substituting eq 7 into eq 6, the distribution of evaporation-induced flow velocity in the NC membrane is simplified to

$$u = u_0\left(1 - \frac{x}{h}\right) \tag{8}$$

where h is the length of the NC membrane.

In addition to pure molecular diffusion, the evaporation-induced flow would cause convective diffusion of the substance in the liquid-filled NC membrane. Therefore, the concentration distribution of the diffusing substance can be described using the convective diffusion equation given as follows

$$\frac{\partial c_A}{\partial t} + u\frac{\partial c_A}{\partial x} = D_{eff}\frac{\partial^2 c_A}{\partial x^2} \tag{9}$$

4. RESULTS AND DISCUSSION

Before studying diffusion in the presence of evaporation, we conducted a series of pure diffusion experiments under RH =

https://doi.org/10.1021/acsomega.1c03052
ACS Omega 2021, 6, 21646−21654

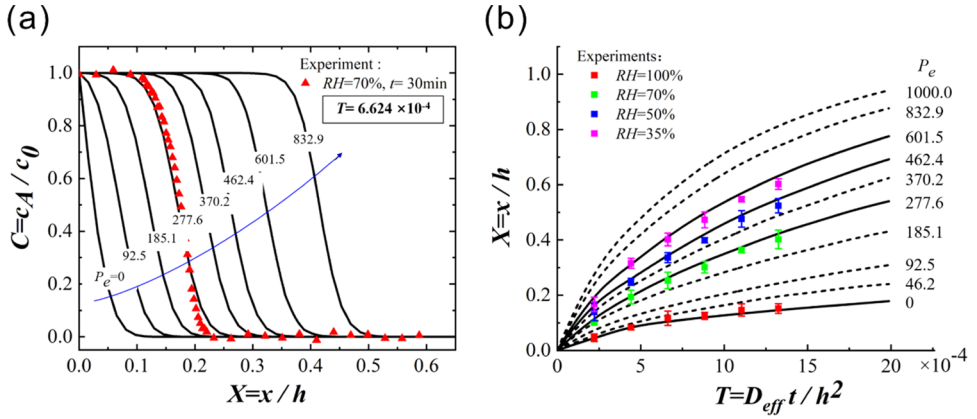

Figure 4. Effect of the Peclet number P_e on diffusion under evaporation: (a) relationship between the dimensionless concentration and the diffusion distance at $T = 6.624 \times 10^{-4}$. (b) Relationship between the dimensionless diffusion distance and time at different values of P_e.

100% to validate the experimental method. The corresponding experimental results are presented in Section 1 of the Supporting Information. It was found that the measured concentration profiles of erioglaucine disodium salt dye along liquid-filled NC membranes are consistent with the classic 1-D diffusion theory without evaporation.

To study how evaporation affects the diffusion behavior of a liquid-filled porous material, we carried out experiments of erioglaucine disodium salt dye diffusion in NC membranes under a wide range of RH, from 35−100%. Figure 3a shows the measured diffusion images of the NC membrane (HFC13502) under selected relative humidities RH = 35, 50, 70, and 100%, at ambient temperature (~21 °C). Figure 3b plots the corresponding diffusion distance as a function of time. Compared to the case of RH = 100%, the diffusion speed is obviously increased under evaporation conditions, and the diffusion speed increases as the RH is decreased. For example, the diffusion distances at RH = 35, 50, and 70% are 3.7, 3.1, and 2.5 times that of the case without evaporation, at the same diffusion time of 3000 s.

In addition to the diffusion speed, evaporation also greatly changes the concentration distribution of the diffusion substance. As shown in Figure 2c, for the case of pure diffusion without evaporation, the concentration profile sharply decreases along the NC membrane from the source. In contrast, in the presence of evaporation, the concentration profile exhibits a platform near the source, followed by a sharp decline after the platform; and the lower the RH, the longer the platform. Such distinct distribution behavior occurs because evaporation induces flow in the NC membrane. With flow velocity in the NC membrane peaking at the source, convective diffusion dominates the migration of erioglaucine disodium salt dye in the membranes near the source. Due to high efficiency of convection transport, the concentration near the source region is only slightly decreased compared with the initial concentration. On the other hand, eq 8 indicates that flow velocity in the NC membrane decreases along the flow direction, thus convection effects diminish gradually along the diffusion direction and molecular diffusion dominates near the diffusion front.

In the presence of evaporation, the classical diffusion theory fails to predict the initial platform of concentration distribution near the source region. With convective effects accounted for, our modified theory successfully predicts the variation of concentration distribution with the diffusion distance relative to experimental observations, as shown in Figure 2c−e.

To find the main influential parameter of the evaporative diffusion process, the governing equation, *i.e.*, eq 9, was normalized as

$$\frac{\partial C}{\partial T} + P_e(1 - X)\frac{\partial C}{\partial X} = \frac{\partial^2 C}{\partial X^2} \tag{10}$$

where the dimensionless concertation, distance, and time were defined as $C = c_A/c_0$, $X = x/h$, and $T = D_{eff}\, t/h^2$ respectively, and $P_e = u_0 t/D_{eff}$ is the Peclet number measuring the relative contribution of convection to molecular diffusion. It can be seen from eq 10 that P_e is the governing parameter of the evaporative diffusion process in liquid-filled porous materials. By numerically solving the abovementioned equation, the effect of P_e on the diffusion process was examined.

Figure 4a presents the dimensionless concentration as a function of the dimensionless diffusion distance with varying P_e numbers, whereas Figure 4b plots the corresponding dimensionless diffusion front as a function of dimensionless time. When P_e is small, the concentration distribution follows the trend of coerror function, where molecular diffusion is dominant and $P_e = 0$ corresponds to the extreme case of diffusion without evaporation. As P_e is increased, the initial platform of the concentration profile near the source becomes more remarkable. At a given diffusion time, the P_e number is proportional to the characteristic velocity u_0 and inversely proportional to the effective diffusion coefficient D_{eff}. The characteristic velocity depends upon the evaporation rate on the surface of a liquid-filled porous material, reflecting the influence of the external environment on the transfer process. The effective diffusion coefficient depends upon the nature of the diffusion substance and the porous material. Therefore, the P_e number reflects the relative contribution of evaporation-induced convection and molecular diffusion to the migration of a substance in a liquid-filled porous material. $P_e = 1$ means that the contribution of evaporative convection equals molecular diffusion. With RH fixed at 100, 70, 50, and 35%, respectively, the convection velocity caused by evaporation was calculated to be 0, 2.5, 4.1, and 5.3 μm/s, corresponding to $P_e = 0$, 278, 462, and 601, respectively. Therefore, under common environmental humidity conditions (35−70%), evaporation diffusion significantly exceeds molecular diffusion. Even when the relative humidity is as high as 95%, the corresponding P_e equals 46 ($u_0 = 0.41$ μm/s), indicating that the effect of

https://doi.org/10.1021/acsomega.1c03052
ACS Omega 2021, 6, 21646−21654

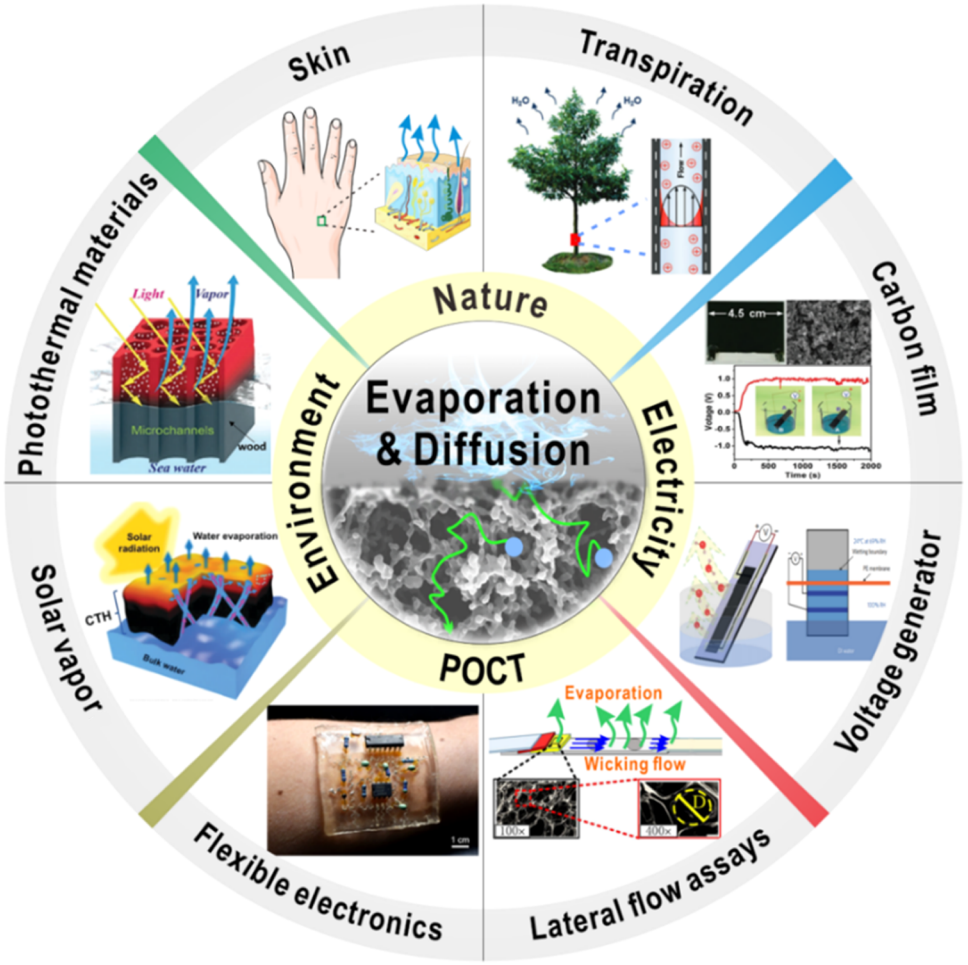

Figure 5. Typical examples related to diffusion in liquid-filled porous materials under evaporation and its wide application in natural and engineering problems, ranging from transpiration of plants[41] (photograph courtesy of Ding, copyright@Wiley, 2017.), the evaporation-induced electric generator[40,41] (photograph courtesy of Xue, copyright@Springer Nature, 2017.), seawater purification[14,48] (photograph courtesy of Zhou, copyright@ Royal Society of Chemistry, 2018. Photograph courtesy of Gao, copyright@ Royal Society of Chemistry, 2019.), flexible electronics[69] (photograph courtesy of Liu, copyright@ Royal Society of Chemistry, 2020.), and paper-based diagnostics[8] (photograph courtesy of Tang, copyright@Springer Nature, 2017.).

evaporation on diffusion is still remarkable. It is worth noting that, in common sense, it is usually believed that the evaporation effect can be ignored if RH is high (*e.g.*, >90%), but our results show that for diffusion in a liquid-filled porous material, the evaporation effect can only be ignored when RH is close to 100%.

Introducing the dimensionless number P_e, we found that evaporation-induced flow in a liquid-filled porous material can achieve a velocity of 0.4−5 μm/s. Evaporation-induced flow and diffusion (EIFD) may be important in both science and engineering, as summarized in Figure 5. From a scientific perspective, EIFD may provide a mechanistic understanding of natural fluid transport, such as microcirculation in living tissues. Living tissue is a liquid-filled porous material composed mainly of cells and extracellular matrices (ECMs), with cells residing in highly specialized ECMs that provide mechanical support to the cells. Interstitial fluid with a composition similar to that of blood plasma flows from capillaries to tissue, finally collected to lymphatic capillaries. Interstitial flow functions not only to transport nutrients and metabolic wastes for cells, but also plays important roles in the morphogenesis, function, and pathogenesis of tissues.[65] Driving forces for such interstitial flow are usually believed to be hydrostatic and osmotic pressure differences between the blood, interstitium, and lymphatics. However, for peripheral tissues, such as the skin that is far away from the heart, the pumping force may be insufficient to drive microcirculation. Given that the interstitial flow velocity is on the order of 0.1−2 μm/s,[65] similar to the evaporation-induced flow velocity (0.4−5 μm/s) in liquid-filled porous materials, we envision that the EIFD mechanism may be an important driving force to induce flow from capillaries to tissues. In addition, evaporation may further affect human health by changing the interstitial fluid pressure, critical for tumor growth[66−68] and ocular health.[65]

From the engineering perspective, the evaporation-induced flow and diffusion (EIFD) phenomenon has been widely utilized in cutting-edge technologies, such as evaporation-induced flow in carbon nanostructures to generate voltage,[40−42] self-powered evaporation-biosensing devices,[43] and seawater purification,[14,48] as shown in Figure 5. However, the flow velocity and the rate of material exchange in liquid-filled porous materials in the abovementioned applications were not quantified. The present model can provide a theoretical basis for predicting the system function such as electricity generation with evaporation conditions in previous studies.[40−42] The EIFD mechanism can further inspire new methods to control

https://doi.org/10.1021/acsomega.1c03052
ACS Omega 2021, 6, 21646−21654

the flow velocity and solute transport in liquid-filled porous materials by adjusting the evaporation rate (*e.g.*, through changing airflow velocity, RH, and temperature). For example, in lateral flow assays, since the driving ability of capillary flow at a later stage is greatly reduced, the signal intensity is limited. By adjusting the evaporation rate, the amount of the sample flowing through the test zone can be controlled to promote bioreactions, which may improve the detection performance.

5. CONCLUSIONS

Evaporation-induced acceleration of diffusion in liquid-filled porous materials was revealed by performing noninvasive diffusion imaging experiments under different relative humidities (RHs). Accelerated diffusion was explained by proposing an underlying physical mechanism that evaporation would induce a weak flow in the liquid-filled porous materials, thus causing convective diffusion, *i.e.*, evaporation-induced flow and diffusion (EIFD). Based on the EIFD mechanism, a convective diffusion model was constructed to quantitatively describe the diffusion behavior in liquid-filled porous materials under evaporation. Acceleration of diffusion due to evaporation was found to be remarkable, for example, at a typical diffusion time of 3000 s, at RH = 70, 50, and 30%, the diffusion front is 3.7, 3.1, and 2.5 times further than the case without evaporation. In addition, evaporation would alter the concentration distribution of the diffusion substance in the liquid-filled porous material. The measured concentration distribution without evaporation conformed to the classical 1-D diffusion theory. However, under evaporation due to linearly decreasing flow velocity along the direction of diffusion, the concentration profile near the source of the concentration exhibited a platform, followed by a rapid drop away from the source. This trend has been successfully predicted by our modified 1-D diffusion theory. Upon normalizing the governing equation, it was shown that the dimensionless number P_e, which measures the relative contribution of the evaporation effect to pure molecular diffusion, is the single parameter dictating the diffusion process under evaporation. At a high RH (*e.g.* RH = 95%), the evaporation effect is usually believed to be negligible. The present analysis nonetheless demonstrated that, in this case (RH = 95%), the P_e number (P_e = 46) was much higher than unity and the evaporation-induced diffusion continued to overwhelm molecular diffusion as at lower RHs. From the engineering perspective, the present study may inspire new control methods for flow and material exchange in a variety of cutting-edge technologies, such as paper-based diagnostics, hydrogel-based flexible electronics, evaporation-induced electricity generation, and seawater purification.

■ ASSOCIATED CONTENT

Supporting Information

The Supporting Information is available free of charge at https://pubs.acs.org/doi/10.1021/acsomega.1c03052.

Experimental results for pure diffusion without evaporation (Section 1) and simulation of the evaporation flux (Section 2) (PDF)

■ AUTHOR INFORMATION

Corresponding Author

Shangsheng Feng − *The Key Laboratory of Biomedical Information Engineering of Ministry of Education, School of Life Science and Technology, Xi'an Jiaotong University, Xi'an 710049, P. R. China; Bioinspired Engineering and Biomechanics Center (BEBC), Xi'an Jiaotong University, Xi'an 710049, P. R. China;* orcid.org/0000-0001-6181-1235; Email: shangshengfeng@xjtu.edu.cn

Authors

Xuefeng Wang − *The Key Laboratory of Biomedical Information Engineering of Ministry of Education, School of Life Science and Technology, Xi'an Jiaotong University, Xi'an 710049, P. R. China; Bioinspired Engineering and Biomechanics Center (BEBC), Xi'an Jiaotong University, Xi'an 710049, P. R. China*

Pengpeng Jia − *The Key Laboratory of Biomedical Information Engineering of Ministry of Education, School of Life Science and Technology, Xi'an Jiaotong University, Xi'an 710049, P. R. China; Bioinspired Engineering and Biomechanics Center (BEBC), Xi'an Jiaotong University, Xi'an 710049, P. R. China*

Shanyouming Sun − *Bioinspired Engineering and Biomechanics Center (BEBC), Xi'an Jiaotong University, Xi'an 710049, P. R. China;* Present Address: State Key Laboratory for Strength and Vibration of Mechanical Structures, Xi'an Jiaotong University, Xi'an 710049, P.R. China; orcid.org/0000-0003-0427-3615

Xiaocong He − *The Key Laboratory of Biomedical Information Engineering of Ministry of Education, School of Life Science and Technology, Xi'an Jiaotong University, Xi'an 710049, P. R. China; Bioinspired Engineering and Biomechanics Center (BEBC), Xi'an Jiaotong University, Xi'an 710049, P. R. China*

Tian Jian Lu − *State Key Laboratory of Mechanics and Control of Mechanical Structures and Nanjing Center for Multifunctional Lightweight Materials and Structures (MLMS), Nanjing University of Aeronautics and Astronautics, Nanjing 210016, P. R. China*

Feng Xu − *The Key Laboratory of Biomedical Information Engineering of Ministry of Education, School of Life Science and Technology, Xi'an Jiaotong University, Xi'an 710049, P. R. China; Bioinspired Engineering and Biomechanics Center (BEBC), Xi'an Jiaotong University, Xi'an 710049, P. R. China;* orcid.org/0000-0003-4351-0222

Complete contact information is available at: https://pubs.acs.org/10.1021/acsomega.1c03052

Notes

The authors declare no competing financial interest.

■ ACKNOWLEDGMENTS

This work was supported by the National Natural Science Foundation of China (51676156, 51206128, 51706178, and 12032010) and by the Open Fund of State Key Laboratory of Mechanics and Control of Mechanical Structures (MCMS-E0219K02 and MCMS-I-0219 K01). The authors would thank Dr. Meng Shi and Dr. Hao Liu for their helpful discussion.

■ NOTATIONS

P_e, Peclet number
RH, relative humidity
d, pore diameter of NC membranes (μm)
λ, molecular mean free path
φ, porosity
τ, tortuosity
$G_{A,}$ gray value at position x and time t

G_0, gray value at the source point
G, gray value of background
t, time (s)
c_A, concentration at position x and time t (mol/m^3)
c_0, concentration at the source point (mol/m^3)
u, velocity in NC membranes (m/s)
u_0, velocity at source (m/s)
w, width of NC membranes (m)
b, thickness of NC membranes (m)
h, length of NC membranes (m)
ρ, water density (kg/m^3)
m_e, evaporation flux (kg/(m^2·s))
c_s, water vapor concentration on the surface of NC membranes (mol/m^3)
c_{oo}, water vapor concentration in air (mol/m^3)
C, dimensionless concentration
X, dimensionless position
T, dimensionless time

REFERENCES

(1) Gibson, L. J.; Ashby, M. F.; Harley, B. A. *Cellular Materials in Nature and Medicine*; Cambridge University Press, 2010.
(2) Tantemsapya, N.; Meegoda, J. N. Estimation of diffusion coefficient of chromium in colloidal silica using digital photography. *Environ. Sci. Technol.* **2004**, *38*, 3950−3957.
(3) Xia, B.; Pan, Z.; Yan, J.; Zhao, C. Mesoscopic exploration on mass transfer in porous thermochemical heat storage materials. *Int. J. Heat Mass Transfer* **2019**, *135*, 52−61.
(4) Chen, H.; Zhang, W.; Zhu, G.; Xie, J.; Chen, X. Rethinking cancer nanotheranostics. *Nat. Rev. Mater.* **2017**, *2*, No. 17024.
(5) Gosset, A.; Oestreicher, V.; Perullini, M.; Bilmes, S. A.; Jobbágy, M.; Dulhoste, S.; Bayard, R.; Durrieu, C. Optimization of sensors based on encapsulated algae for pesticide detection in water. *Anal. Methods* **2019**, *11*, 6193−6203.
(6) Liu, D.; Kotsmar, C.; Nguyen, F.; Sells, T.; Taylor, N.; Prausnitz, J.; Radke, C. Macromolecule sorption and diffusion in HEMA/MAA hydrogels. *Ind. Eng. Chem. Res.* **2013**, *52*, 18109−18120.
(7) Martinez, A. W.; Phillips, S. T.; Whitesides, G. M. Three-dimensional microfluidic devices fabricated in layered paper and tape. *Proc. Natl. Acad. Sci. U.S.A.* **2008**, *105*, 19606−19611.
(8) Tang, R.; Yang, H.; Gong, Y.; Liu, Z.; Li, X.; Wen, T.; Qu, Z.; Zhang, S.; Mei, Q.; Xu, F. Improved analytical sensitivity of lateral flow assay using sponge for HBV nucleic acid detection. *Sci. Rep.* **2017**, *7*, No. 1360.
(9) Gasperino, D.; Baughman, T.; Hsieh, H. V.; Bell, D.; Weigl, B. H. Improving lateral flow assay performance using computational modeling. *Annu. Rev. Anal. Chem.* **2018**, *11*, 219−244.
(10) Shannon, M. A.; Bohn, P. W.; Elimelech, M.; Georgiadis, J. G.; Marinas, B. J.; Mayes, A. M. Science and technology for water purification in the coming decades. *Nature* **2008**, *452*, 301−310.
(11) Berek, D. Size exclusion chromatography−a blessing and a curse of science and technology of synthetic polymers. *J. Sep. Sci.* **2010**, *33*, 315−335.
(12) Zhang, Y. S.; Choi, S.-W.; Xia, Y. Inverse opal scaffolds for applications in regenerative medicine. *Soft Matter* **2013**, *9*, 9747−9754.
(13) Morrow, N. R.; Mason, G. Recovery of oil by spontaneous imbibition. *Curr. Opin. Colloid Interface Sci.* **2001**, *6*, 321−337.
(14) Zhou, X.; Zhao, F.; Guo, Y.; Zhang, Y.; Yu, G. A hydrogel-based antifouling solar evaporator for highly efficient water desalination. *Energy Environ. Sci.* **2018**, *11*, 1985−1992.
(15) Ehtesabi, H.; Ahadian, M. M.; Taghikhani, V.; Ghazanfari, M. H. Enhanced heavy oil recovery in sandstone cores using TiO_2 nanofluids. *Energy Fuels* **2014**, *28*, 423−430.
(16) Berlin, J. M.; Yu, J.; Lu, W.; Walsh, E. E.; Zhang, L.; Zhang, P.; Chen, W.; Kan, A. T.; Wong, M. S.; Tomson, M. B.; Tour, J. M. Engineered nanoparticles for hydrocarbon detection in oil-field rocks. *Energy Environ. Sci.* **2011**, *4*, 505−509.
(17) He, X.; Guo, Y.; Li, M.; Pan, N.; Wang, M. Effective gas diffusion coefficient in fibrous materials by mesoscopic modeling. *Int. J. Heat Mass Transfer* **2017**, *107*, 736−746.
(18) Bird, R. B.; Stewart, W. E.; Lightfoot, E. N. *Transport Phenomena*; John Wiley & Sons, 2006.
(19) Raccis, R.; Nikoubashman, A.; Retsch, M.; Jonas, U.; Koynov, K.; Butt, H.-J.; Likos, C. N.; Fytas, G. Confined diffusion in periodic porous nanostructures. *ACS Nano* **2011**, *5*, 4607−4616.
(20) Lutz, C.; Kollmann, M.; Bechinger, C. Single-file diffusion of colloids in one-dimensional channels. *Phys. Rev. Lett.* **2004**, *93*, No. 026001.
(21) Cherdhirankorn, T.; Harmandaris, V.; Juhari, A.; Voudouris, P.; Fytas, G.; Kremer, K.; Koynov, K. Fluorescence correlation spectroscopy study of molecular probe diffusion in polymer melts. *Macromolecules* **2009**, *42*, 4858−4866.
(22) Bauer, M.; Godec, A.; Metzler, R. Diffusion of finite-size particles in two-dimensional channels with random wall configurations. *Phys. Chem. Chem. Phys.* **2014**, *16*, 6118−6128.
(23) Yang, S. Y.; Yang, J.-A.; Kim, E.-S.; Jeon, G.; Oh, E. J.; Choi, K. Y.; Hahn, S. K.; Kim, J. K. Single-file diffusion of protein drugs through cylindrical nanochannels. *ACS Nano* **2010**, *4*, 3817−3822.
(24) Icardi, M.; Boccardo, G.; Marchisio, D. L.; Tosco, T.; Sethi, R. Pore-scale simulation of fluid flow and solute dispersion in three-dimensional porous media. *Phys. Rev. E* **2014**, *90*, No. 013032.
(25) Samprovalaki, K.; Robbins, P.; Fryer, P. Investigation of the diffusion of dyes in agar gels. *J. Food Eng.* **2012**, *111*, 537−545.
(26) Perullini, M.; Jobbágy, M.; Japas, M. L.; Bilmes, S. A. New method for the simultaneous determination of diffusion and adsorption of dyes in silica hydrogels. *J. Colloid Interface Sci.* **2014**, *425*, 91−95.
(27) Zürner, A.; Kirstein, J.; Döblinger, M.; Bräuchle, C.; Bein, T. Visualizing single-molecule diffusion in mesoporous materials. *Nature* **2007**, *450*, 705−708.
(28) Skaug, M. J.; Wang, L.; Ding, Y.; Schwartz, D. K. Hindered nanoparticle diffusion and void accessibility in a three-dimensional porous medium. *ACS Nano* **2015**, *9*, 2148−2156.
(29) Kirstein, J.; Platschek, B.; Jung, C.; Brown, R.; Bein, T.; Bräuchle, C. Exploration of nanostructured channel systems with single-molecule probes. *Nat. Mater.* **2007**, *6*, 303−310.
(30) Lee, S. M.; Park, I. K.; Kim, Y. S.; Kim, H. J.; Moon, H.; Mueller, S.; Jeong, Y.-I. Physical, morphological, and wound healing properties of a polyurethane foam-film dressing. *Biomater. Res.* **2016**, *20*, No. 15.
(31) Ahmad, A. L.; Low, S. C.; Shukor, S. R. A.; Fernando, W. J. N.; Ismail, A. Hindered diffusion in lateral flow nitrocellulose membrane: Experimental and modeling studies. *J. Membr. Sci.* **2010**, *357*, 178−184.
(32) Li, Z.; Pollack, G. H. Surface-induced flow: A natural microscopic engine using infrared energy as fuel. *Sci. Adv.* **2020**, *6*, No. eaba0941.
(33) Liu, M.; Wu, J.; Gan, Y.; Hanaor, D. A. H.; Chen, C. Q. Evaporation limited radial capillary penetration in porous media. *Langmuir* **2016**, *32*, 9899−9904.
(34) Moon, B.-U.; Malic, L.; Morton, K.; Jeyhani, M.; Elmanzalawy, A.; Tsai, S. S. H.; Veres, T. Evaporation-driven water-in-water droplet formation. *Langmuir* **2020**, *36*, 14333−14341.
(35) Majhy, B.; Sen, A. K. Evaporation-induced transport of a pure aqueous droplet by an aqueous mixture droplet. *Phys. Fluids* **2020**, *32*, No. 032003.
(36) Cira, N. J.; Benusiglio, A.; Prakash, M. Vapour-mediated sensing and motility in two-component droplets. *Nature* **2015**, *519*, 446−450.
(37) Yunker, P. J.; Still, T.; Lohr, M. A.; Yodh, A. G. Suppression of the coffee-ring effect by shape-dependent capillary interactions. *Nature* **2011**, *476*, 308−311.
(38) Tan, H. Absorption of picoliter droplets by thin porous substrates. *AIChE J.* **2017**, *63*, 1690−1703.

https://doi.org/10.1021/acsomega.1c03052
ACS Omega 2021, 6, 21646−21654

(39) Clarke, A.; Blake, T. D.; Carruthers, K.; Woodward, A. Spreading and imbibition of liquid droplets on porous surfaces. *Langmuir* **2002**, *18*, 2980−2984.
(40) Xue, G. B.; Xu, Y.; Ding, T. P.; Li, J.; Yin, J.; Fei, W. W.; Cao, Y. Z.; Yu, J.; Yuan, L. Y.; Gong, L.; Chen, J.; Deng, S. Z.; Zhou, J.; Guo, W. L. Water-evaporation-induced electricity with nanostructured carbon materials. *Nat. Nanotechnol.* **2017**, *12*, 317−321.
(41) Ding, T.; Liu, K.; Li, J.; Xue, G.; Chen, Q.; Huang, L.; Hu, B.; Zhou, J. All-printed porous carbon film for electricity generation from evaporation-driven water flow. *Adv. Funct. Mater.* **2017**, *27*, No. 1700551.
(42) Zhang, S.; Chu, W.; Li, L.; Guo, W. Voltage distribution in porous carbon black films induced by water evaporation. *J. Phys. Chem. C* **2021**, *125*, 8959−8964.
(43) Guan, H.; Zhong, T.; He, H.; Zhao, T.; Xing, L.; Zhang, Y.; Xue, X. A self-powered wearable sweat-evaporation-biosensing analyzer for building sports big data. *Nano Energy* **2019**, *59*, 754−761.
(44) Zhou, T.; Xin, P.; Li, L.; Barry, D. A.; Simunek, J. Effects of large macropores on soil evaporation in salt marshes. *J. Hydrol.* **2020**, *584*, No. 124754.
(45) Zhou, X. Y.; Guo, Y. H.; Zhao, F.; Yu, G. H. Hydrogels as an Emerging Material Platform for Solar Water Purification. *Acc. Chem. Res.* **2019**, *52*, 3244−3253.
(46) Zhao, F.; Zhou, X.; Shi, Y.; Qian, X.; Alexander, M.; Zhao, X.; Mendez, S.; Yang, R.; Qu, L.; Yu, G. Highly efficient solar vapour generation via hierarchically nanostructured gels. *Nat. Nanotechnol.* **2018**, *13*, 489−495.
(47) He, S.; Chen, C.; Kuang, Y.; Mi, R.; Liu, Y.; Pei, Y.; Kong, W.; Gan, W.; Xie, H.; Hitz, E.; Jia, C.; Chen, X.; Gong, A.; Liao, J.; Li, J.; Ren, Z. J.; Yang, B.; Das, S.; Hu, L. Nature-inspired salt resistant bimodal porous solar evaporator for efficient and stable water desalination. *Energy Environ. Sci.* **2019**, *12*, 1558−1567.
(48) Gao, M.; Zhu, L.; Peh, C. K.; Ho, G. W. Solar absorber material and system designs for photothermal water vaporization towards clean water and energy production. *Energy Environ. Sci.* **2019**, *12*, 841−864.
(49) Wu, L.; Dong, Z.; Cai, Z.; Ganapathy, T.; Fang, N. X.; Li, C.; Yu, C.; Zhang, Y.; Song, Y. Highly efficient three-dimensional solar evaporator for high salinity desalination by localized crystallization. *Nat. Commun.* **2020**, *11*, No. 521.
(50) Chen, F.; Zhou, D.; Wang, J.; Li, T.; Zhou, X.; Gan, T.; Handschuh-Wang, S.; Zhou, X. Rational fabrication of anti-freezing, non-drying tough organohydrogels by one-pot solvent displacement. *Angew. Chem., Int. Ed.* **2018**, *57*, 6568−6571.
(51) Bai, Y.; Chen, B.; Xiang, F.; Zhou, J.; Wang, H.; Suo, Z. Transparent hydrogel with enhanced water retention capacity by introducing highly hydratable salt. *Appl. Phys. Lett.* **2014**, *105*, No. 151903.
(52) Van Engeland, C.; Haut, B.; Spreutels, L.; Sobac, B. Evaporation versus imbibition in a porous medium. *J. Colloid Interface Sci.* **2020**, *576*, 280−290.
(53) Liu, Z.; Hu, J.; Zhao, Y.; Qu, Z.; Xu, F. Experimental and numerical studies on liquid wicking into filter papers for paper-based diagnostics. *Appl. Therm. Eng.* **2015**, *88*, 280−287.
(54) Chang, S.; Kim, W. Dynamics of water imbibition through paper with swelling. *J. Fluid Mech.* **2020**, *892*, No. A39.
(55) Choi, J. R.; Hu, J.; Feng, S.; Abas, W. A. B. W.; Pingguan-Murphy, B.; Xu, F. Sensitive biomolecule detection in lateral flow assay with a portable temperature-humidity control device. *Biosens. Bioelectron.* **2016**, *79*, 98−107.
(56) Sun, S.; Feng, S.; Ji, C.; Shi, M.; He, X.; Xu, F.; Lu, T. J. Microstructural effects on permeability of Nitrocellulose membranes for biomedical applications. *J. Membr. Sci.* **2020**, *595*, No. 117502.
(57) Wong, R.; Tse, H. *Lateral Flow Immunoassay*; Springer Science & Business Media: 2008.
(58) Samprovalaki, K.; Fryer, P. J. Development of an experimental procedure for real time investigation of diffusion in foods. *Sens. & Instrumen. Food Qual. Safety* **2011**, *5*, 78−89.
(59) Ray, E.; Bunton, P.; Pojman, J. A. Determination of the diffusion coefficient between corn syrup and distilled water using a digital camera. *Am. J. Phys.* **2007**, *75*, 903−906.
(60) Crank, J. *Mathematics of Diffusion*; Oxford University Press, 1979.
(61) Pradhan, T. K.; Panigrahi, P. K. Unexpectedly absence of Marangoni convection in an evaporating water meniscus. 2020, arXiv:2004.01730. arXiv.org e-Print archive. https://arxiv.org/abs/2004.01730.
(62) Pradhan, T. K.; Panigrahi, P. K. Condensation induced internal convection of two neighboring droplets. 2020, arXiv:2003.09013. arXiv.org-e-Print-archive.https://arxiv.org/abs/2003.090132020.
(63) Li, Y.; Lv, P.; Diddens, C.; Tan, H.; Wijshoff, H.; Versluis, M.; Lohse, D. Evaporation-Triggered Segregation of Sessile Binary Droplets. *Phys. Rev. Lett.* **2018**, *120*, No. 224501.
(64) Diddens, C.; Tan, H.; Lv, P.; Versluis, M.; Kuerten, J. G. M.; Zhang, X.; Lohse, D. Evaporating pure, binary and ternary droplets: thermal effects and axial symmetry breaking. *J. Fluid Mech.* **2017**, *823*, 470−497.
(65) Swartz, M. A.; Fleury, M. E. Interstitial flow and its effects in soft tissues. *Annu. Rev. Biomed. Eng.* **2007**, *9*, 229−256.
(66) Sarntinoranont, M.; Rooney, F.; Ferrari, M. Interstitial stress and fluid pressure within a growing tumor. *Ann. Biomed. Eng.* **2003**, *31*, 327−335.
(67) Anderson, A. R. A.; Weaver, A. M.; Cummings, P. T.; Quaranta, V. Tumor morphology and phenotypic evolution driven by selective pressure from the microenvironment. *Cell* **2006**, *127*, 905−915.
(68) Ozturk, D.; Yonucu, S.; Yilmaz, D.; Unlu, M. B. Influence of vascular normalization on interstitial flow and delivery of liposomes in tumors. *Phys. Med. Biol.* **2015**, *60*, 1477−1496.
(69) Liu, H.; Li, M. X.; Liu, S. B.; Jia, P. P.; Guo, X. J.; Feng, S. S.; Lu, T. J.; Yang, H. Y.; Li, F.; Xu, F. Spatially modulated stiffness on hydrogels for soft and stretchable integrated electronics. *Mater. Horiz.* **2020**, *7*, 203−213.

https://doi.org/10.1021/acsomega.1c03052
ACS Omega 2021, 6, 21646−21654